Research Square

Preprints are preliminary reports that have not undergone peer review.
They should not be considered conclusive, used to inform clinical practice,
or referenced by the media as validated information.

Gill and liver transcriptomes reveal tissue-specific metabolic and immune responses to acute salinity reduction in juvenile yellowfin tuna

Ziyi Jiang
South China Sea Fisheries Research Insitute
Zhengyi Fu
South China Sea Fisheries Research Insitute
Junhua Huang
Sanya Tropical Fisheries Research Institute
Dianchang Zhang
South China Sea Fisheries Research Insitute
Xuxiong Huang
Shanghai Ocean University
Rui Yang
South China Sea Fisheries Research Insitute
Jing Hu
South China Sea Fisheries Research Insitute
Zhiyong Jiang
Agro Tech Extension Center of Guangdong Province
Zhenhua Ma
zhenhua.ma@foxmail.com

South China Sea Fisheries Research Insitute

Research Article

Keywords: Thunnus albacares, comparative transcriptomics, low salinity, gill, liver, energy metabolism, protein homeostasis, immune response, RNA-seq

Posted Date: November 20th, 2026

DOI: https://doi.org/10.21203/rs.3.rs-11496358/v1

License: This work is licensed under a Creative Commons Attribution 4.0 International License.
Read Full License

Additional Declarations: No competing interests reported.

Gill and liver transcriptomes reveal tissue-specific metabolic and immune responses to acute salinity reduction in juvenile yellowfin tuna

Ziyi Jiang[1,2,3], Zhengyi Fu[1,2,3], Junhua Huang[2,3], Dianchang Zhang[1], Xuxiong Huang[4], Rui Yang[1,2,3], Jing Hu[1,2,3], Zhiyong Jiang[5], Zhenhua Ma[1,2,3*]

1 South China Sea Fisheries Research Institute, Chinese Academy of Fishery Sciences, Guangzhou 510300, China

2 Key Laboratory of Efficient Utilization and Processing of Marine Fishery Resources of Hainan Province, Sanya Tropical Fisheries Research Institute, Sanya 572018, China

3 Hainan Fisheries Innovation Research Institute, Chinese Academy of Fishery Sciences, Sanya 572024, China

4 Research Centre of the Ministry of Agriculture and Rural Affairs on Environmental Ecology and Fish Nutrition, Shanghai Ocean University, Shanghai 201306, China

5 Agro-Tech Extension Center of Guangdong Province, Guangzhou 510520, China

*Correspondence: zhenhua.ma@foxmail.com

Abstract

Background: Salinity changes alter the osmotic environment of marine fishes, but the transcriptional responses of different organs can follow distinct trajectories. In juvenile yellowfin tuna (*Thunnus albacares*), the temporal relationships among metabolic, protein-homeostasis and immune-related responses remain incompletely characterized. We compared gill and liver transcriptomes after 6, 24 and 48 h at 29‰ with tissue-specific baselines collected at 0 h in 32‰ seawater. Twenty-four RNA-seq libraries represented three tank-level biological replicates per tissue and sampling point.

Results: Differential-expression analysis identified 559, 2,548 and 3,485 differentially expressed genes in gill at 6, 24 and 48 h, respectively, and 333, 717 and 626 in liver. Ranked gene-set enrichment revealed sustained positive enrichment of branchial oxidative phosphorylation and protein homeostasis, with increasingly prominent translation-related responses at 24 and 48 h. Several branchial immune-related gene sets were negatively enriched at the later times. Liver showed early positive enrichment of protein processing and glycosylation, over-representation of bacterial- and viral-defence terms among 24 h-specific genes, and positive enrichment of oxidative phosphorylation and translation at 48 h. The later hepatic profile also

included negative enrichment of fatty-acid degradation and endoplasmic-reticulum protein processing. Temporal intersections identified 140 gill and 26 liver genes that were differentially expressed in the same direction at all three times. qRT-PCR profiles for eight selected genes broadly agreed with the RNA-seq trends.

Conclusions: The gill and liver exhibited distinct transcriptional trajectories during acute low-salinity exposure, combining a persistent branchial metabolic signature with successive hepatic changes in protein processing, immunity and energy metabolism. This comparative transcriptomic analysis identifies sustained and time-specific gene responses and prioritizes pathways for investigating the molecular basis of salinity responses in juvenile yellowfin tuna.

Keywords: *Thunnus albacares*; comparative transcriptomics; low salinity; gill; liver; energy metabolism; protein homeostasis; immune response; RNA-seq

Introduction

Changes in environmental salinity require marine fishes to adjust water and ion exchange while maintaining cellular function. Rainfall, river discharge and water-mass exchange can freshen coastal and surface waters, and long-term changes in ocean salinity reflect changes in the global water cycle [1]. These changes alter the osmotic gradients across exposed epithelia, linking ion transport to the metabolic and protein-maintenance processes that support it [2-4]. The response also depends on physiological plasticity and exposure duration [5]. Transcriptomic comparisons across organs and sampling times can help resolve how these processes are organized during acute salinity reduction, including the immune-related responses that accompany metabolic adjustment.

The gill and liver provide complementary perspectives on this response. The gill couples direct environmental exposure to gas exchange, ion regulation, acid-base balance and nitrogen excretion [2,3]. Changes in its transport machinery involve energy metabolism, membrane-protein maintenance and protection of the epithelial interface. Experiments in tilapia have linked branchial transport and metabolic gene expression to salinity-dependent differences in metabolic rate [6], while studies in tilapia and milkfish implicate protein quality control in branchial osmotic responses [7,8]. Salinity can also affect fish growth through changes in metabolic expenditure and energy use [9]. The liver integrates substrate metabolism and

protein production. Hepatic responses to salinity include changes in carbohydrate, amino-acid and lipid metabolism, with the pattern depending on species and exposure conditions [10-13].

Immune-related gene expression provides another dimension of the salinity response. The gill regulates ions at an interface exposed to environmental microbes, whereas the liver contributes circulating immune factors and systemic defence [14-17]. Salinity-responsive transcriptomes in teleosts show changes in immune pathways alongside transport and metabolic functions [14,16,17]. Cell-resolved work in scallop heart has likewise identified heterogeneous metabolic and immune-associated responses during heat stress [18], illustrating that environmental responses depend on the biological compartment examined. For gill and liver, comparing the direction and timing of pathway enrichment can distinguish shared functional themes from organ-specific responses and identify when metabolic and immune-related transcription changes concurrently.

Temporal sampling is essential for interpreting these gene-expression patterns. Transcriptomic studies of osmotic acclimation have described early sensing and signalling followed by changes in effector proteins and cellular maintenance [19,20]. Comparative work in killifish has linked differences in hypoosmotic tolerance to distinct acute and acclimatory expression responses [21], while studies in other teleosts have established organ-specific metabolic and stress-related signatures [17,22,23]. These findings leave unresolved how persistent and transient transcriptional components are distributed between gill and liver in juvenile yellowfin tuna. Examining successive exposure times allows genes that consistently meet differential-expression criteria to be distinguished from those detected at individual stages, while ranked pathway analysis captures coordinated expression changes across larger gene sets.

Yellowfin tuna (*Thunnus albacares*) provides a distinctive context for examining these responses because its sustained swimming is associated with high metabolic demand [24]. Previous experiments in juveniles exposed to a reduction from 32‰ to 29‰ documented changes in antioxidant indices and digestive physiology [25,26]. The accompanying gene-expression patterns across gill and liver remain less well resolved. Characterizing these patterns can connect the physiological observations to mitochondrial metabolism, protein homeostasis and immune-related transcription. Because the challenge remains within marine salinity conditions, the resulting profiles also provide a basis for comparison with the larger osmotic transitions commonly examined in euryhaline fishes.

Here, we compared gill and liver transcriptomes after 6, 24 and 48 h of exposure to 29‰ seawater with tissue-specific baselines collected at 0 h in 32‰ seawater. We asked which metabolic and immune-related gene programs characterized each organ, how their enrichment changed across the exposure series, and which genes responded consistently at all three times. Differential-expression analysis, ranked gene-set enrichment and temporal intersections were combined to resolve gene-level and pathway-level responses. Co-expression analysis described covariation among persistent genes, and qRT-PCR assessed the expression trends of eight selected targets. This approach identifies candidate genes and pathways for subsequent functional investigation within a comparative account of the two organs.

Methods

Experimental animals and salinity exposure

The experimental design followed the salinity challenge described by Zhou et al. [26]. The experiment was conducted at the Lingshui Research Station of the Tropical Fisheries Research and Development Center, South China Sea Fisheries Research Institute, Chinese Academy of Fishery Sciences. Seventy-two juvenile yellowfin tuna (standard length 28.97 ± 2.17 cm; body mass 646.52 ± 66.32 g) were randomly distributed among six 5,000-L fiberglass tanks (12 fish per tank) after a 7-day acclimation. Fish were fed fresh miscellaneous fish (approximately 4 cm × 2 cm pieces) from 08:30 to 09:00 h to apparent satiety (5-8% body mass per day) and were fasted for 24 h before salinity adjustment and during the exposure. Three tanks remained at 32‰ and three were reduced to 29‰ by adding tap water aerated for 24 h at 1‰ per h. Exposure time was measured from the point at which the treatment tanks reached 29‰. Water exchange was approximately 300% tank volume per day; photoperiod was 14 h light:10 h dark; temperature was 29.5 ± 0.5 °C; dissolved oxygen was >7.5 mg L^{-1}; pH was 7.93 ± 0.12; ammonia nitrogen was <0.10 mg L^{-1}; and nitrite nitrogen was <0.05 mg L^{-1}. Salinity, temperature, dissolved oxygen and pH were monitored with an HQ40d portable meter, and ammonia and nitrite were measured with commercial test kits.

At 0 h, three fish were randomly sampled from each of the three 32‰ control tanks. Three fish were then sampled from each 29‰ tank at 6, 24 and 48 h. Fish were euthanized with an overdose of AQUI-S (100 mg L^{-1}). Gill and liver were dissected on ice, frozen in liquid nitrogen and stored at −80 °C. For each tissue, samples from the three fish collected from the same tank were pooled to generate one RNA-seq library, with the tank pool treated as the biological replicate. The three baseline libraries originated from separate control

tanks, and each low-salinity time point comprised one pooled library from each treatment tank. Because RNA-seq libraries from control fish were available only at 0 h, these pools served as the common baseline for all low-salinity comparisons. The animal study protocol was approved by the Animal Care and Use Committee of the South China Sea Fisheries Research Institute, Chinese Academy of Fishery Sciences (BIOL5346, 9 May 2022).

RNA extraction, library preparation and sequencing

Total RNA was extracted with TRIzol reagent according to the manufacturer's instructions. RNA concentration and purity were measured with a NanoDrop spectrophotometer, and integrity was assessed by agarose-gel electrophoresis and an Agilent 2100 Bioanalyzer. Poly(A)-selected libraries were prepared with the TruSeq RNA Sample Preparation Kit and sequenced as paired-end reads on an Illumina HiSeq X Ten platform. Per-library sequencing-quality metrics are reported in Table S1.

Sequencing quality was high across all 24 libraries: Q20 values ranged from 94.91% to 96.18%, and Q30 values ranged from 89.35% to 91.44%.

qRT-PCR target selection and primer design

Eight genes were selected to represent functional themes identified by RNA-seq: *atp5l* (NCBI symbol *atp5mg*), mitochondrial ATP production; *blmh*, proteolysis and amino-acid metabolism; *hspa8b*, protein chaperoning; *sod1*, antioxidant defence; *apoeb*, lipid transport; *b2m*, major histocompatibility complex class I antigen presentation; *usp18*, interferon-associated immune regulation and deubiquitination; and *dmgdh*, dimethylglycine and one-carbon metabolism. In the RNA-seq data, *usp18* was consistently upregulated in gill and was a highly connected member of the persistent-gene co-expression network, whereas *dmgdh* was consistently downregulated in liver. Primers were designed using NCBI against the listed *Thunnus albacares* RefSeq mRNA accessions (Table 1).

Table 1. Primer sequences, RefSeq accessions and expected amplicon sizes for qRT-PCR assays.

Gene abbreviation	Primer sequence (5′-3′)	Amplicon size (bp)	Accession number
atp5l	F: CCATCGAGGGAGCCACAAAT R: CCGTTCCTTAGAGCATCCTTCA	85	XM_044371713.1
blmh	F: TTCTCGTGCCTCAACGTCAT R: AGTAGCAACGCTCAACCTTGT	112	XM_044353709.1
hspa8b	F: GACCGACAAACGGACTGACG R: CTTGGACATGGCTCCTCCGT	142	XM_044353616.1
sod1	F: GCCGGTCCTAATGATGCAGA R: TCAGCCTTCTCATGGATCACC	158	XM_044369869.1
apoeb	F: CTGAGGAGATCCGCAACACT R: CTGGCCTGATTGACGTAGGG	112	XM_044360326.1
b2m	F: GACTATGCCTGGGAGCCAAA R: CCGGGAGAAACTGTGATCCTT	122	XM_044344086.1
usp18	F: GCCAGCTAACCACCATGACT R: GGATGTCAAGAGCCAGTGCT	146	XM_044342607.1
dmgdh	F: CAAACTGAACAAGCCGGGTG R: GTCGTGTTACCGACCACCTT	165	XM_044333770.1

For comparison with RNA-seq, glyceraldehyde-3-phosphate dehydrogenase (GAPDH) served as the reference transcript and the 0 h samples served as the calibrator. Relative transcript abundance was calculated with the comparative Ct method ($2^{-\Delta\Delta CT}$) [27], normalized to a 0 h value of 1, and summarized as the mean ± standard deviation (SD) across three independent tank samples. RNA-seq and qRT-PCR fold changes were displayed as paired bars on a common scale for each gene, with SD error bars for qRT-PCR only (Figures S4 and S5).

Gene quantification and statistical analysis

Adapters and low-quality bases were removed with Trimmomatic v0.39, and filtered reads were aligned to the yellowfin tuna reference genome assembly fThuAlb1.1 (GCF_914725855.1; NCBI Release 100) with HISAT2 v2.2.1 [28,29]. Gene-level abundance was estimated with StringTie v2.1.7 [30], yielding counts for 36,407 unique genes across 24 libraries. Differential expression was analysed with DESeq2. Analyses were conducted in R 4.5.3 with DESeq2 1.50.2 [31]. For each tissue and time point, genes with at least 10 counts in at least three of the six libraries were retained. A negative-binomial model with condition as its sole design term estimated expression at 29‰ relative to the tissue-specific 0 h baseline. Because each pairwise contrast contained one library from each tank, no repeated-tank term was included. DESeq2 median-of-ratios normalization, dispersion estimation, independent filtering and two-sided Wald tests were used. P values were adjusted by the Benjamini-Hochberg (BH) method within each contrast to control the false discovery rate (FDR) [32]. Differentially expressed genes (DEGs) were defined by adjusted $P < 0.05$ and absolute log2 fold change > 1. Sensitivity analyses also applied no fold-change threshold or an absolute log2 fold-change threshold > 2.

Each exposure time was compared separately with the 0 h baseline to estimate expression differences at each sampling point. As a sensitivity analysis, a four-level condition model was also fitted to all 12 libraries within each tissue. The pairwise and four-level models yielded nearly identical log2 fold-change estimates (Spearman $\rho = 0.9999$ for every contrast) and highly correlated Wald statistics ($\rho = 0.990$-0.996), although the number of genes meeting both the FDR and effect-size criteria differed. Results reported in the main text are from the pairwise models.

Expression visualization and functional enrichment analysis

Variance-stabilized counts were used for principal component analysis (PCA), sample-distance matrices and heatmaps. PCA included all filtered genes and the 12 libraries from each tissue. Additional PCA and sample-distance diagnostics are shown in Figure S1. For each contrast, heatmaps show the 30 DEGs with the smallest adjusted P values, with expression standardized by gene across the six libraries. Temporal overlap was assessed using gene identifiers. Genes that met the DEG criteria at all three exposure times and had concordant log2 fold-change signs were classified as persistent.

Genes were assigned to Gene Ontology (GO) terms and Kyoto Encyclopedia of Genes and Genomes (KEGG) pathways [33,34]. For over-representation analysis (ORA), the background comprised genes with finite adjusted P values in the corresponding contrast and functional database. Analysis of persistent DEGs used genes testable in all three contrasts, whereas analysis of time-specific DEGs used the background for the corresponding contrast. Terms containing 5-500 background genes were tested, and P values were adjusted by the Benjamini-Hochberg and Bonferroni methods. Preranked gene set enrichment analysis (GSEA) used finite DESeq2 Wald statistics and gene sets containing 15-500 mapped genes and was run with fgseaMultilevel (eps = 0; nPermSimple = 10,000) [35,36]. Benjamini-Hochberg adjustment was applied separately within each tissue, time point and database. Exact ties were ordered by gene identifier. Figures distinguish FDR-supported results from nominal associations. Figures S2 and S3 summarize GO and KEGG over-representation results for each tissue and sampling time.

For each tissue, Spearman correlations were calculated across the 12 variance-stabilized libraries for genes classified as persistent. Edges with absolute $\rho \geq 0.80$ were included, and node degree was calculated from the complete tissue network. The five highest-degree upregulated and downregulated genes were selected for display; ties were ordered by gene identifier. The networks were treated as descriptive summaries of covariation, and no edge-level significance testing or regulatory inference was applied.

Results

Experimental design and RNA-seq comparisons

For each tissue, three tank-level samples collected in 32‰ seawater at 0 h served as the baseline for comparisons with samples collected after 6, 24 or 48 h at 29‰ (Figure 1a). Each RNA-seq library comprised tissue pooled from three fish within one tank, and the tank pool was treated as the biological replicate. Figure 1b summarizes the numbers of upregulated and downregulated genes identified in each comparison.

Table 2. Differential-expression summary for each low-salinity group relative to the 0 h baseline.

Tissue	Time	Genes tested	DEGs	Up	Down	DEGs, |log2FC| > 2
Gill	6 h	19,419	559	208	351	161
Gill	24 h	19,183	2,548	1,669	879	307
Gill	48 h	19,066	3,485	1,599	1,886	897
Liver	6 h	12,643	333	135	198	122
Liver	24 h	12,746	717	360	357	259
Liver	48 h	12,458	626	352	274	225

DEGs were defined by a Benjamini-Hochberg adjusted $P < 0.05$ and an absolute log2 fold change > 1. A more stringent absolute log2 fold-change threshold of 2 was also evaluated. Each tissue and exposure time was analysed independently relative to its 0 h baseline.

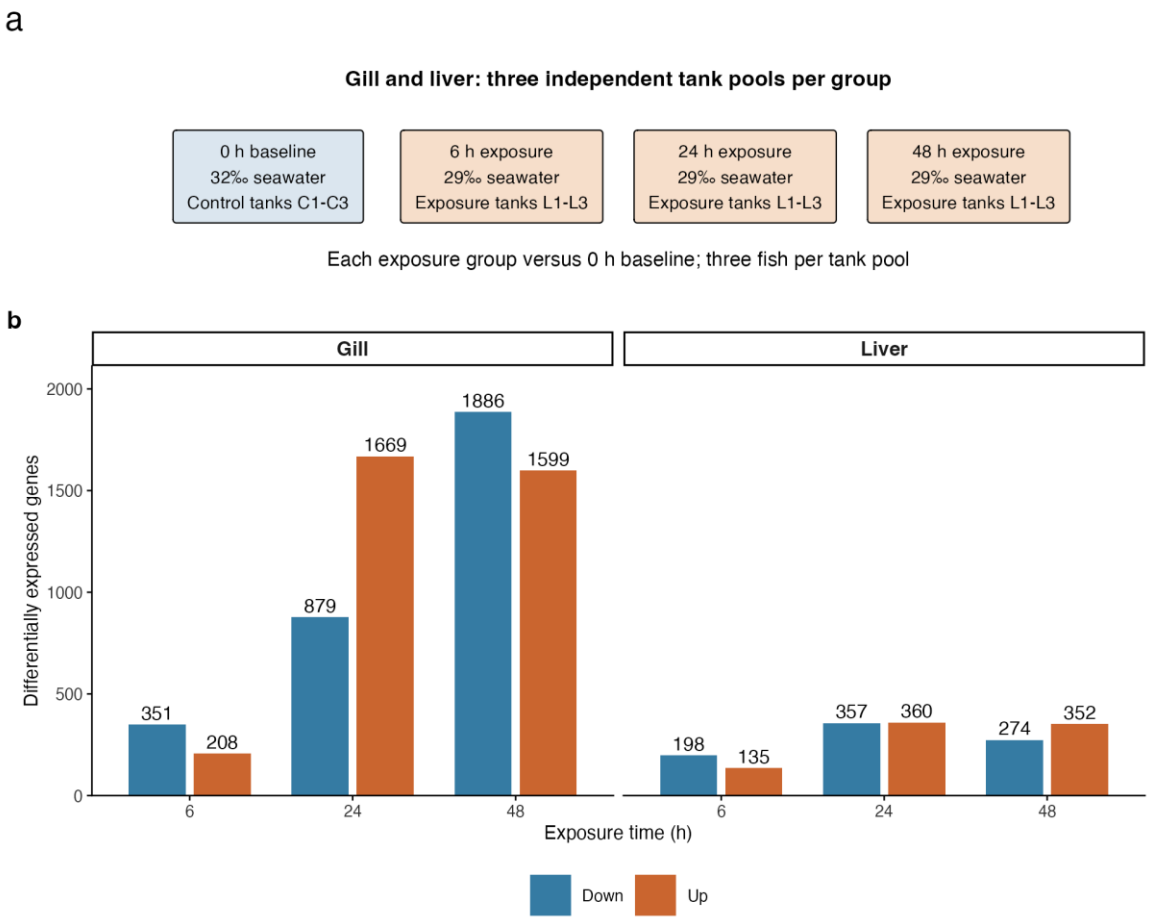

Figure 1. Experimental design and numbers of differentially expressed genes. (a) Seventy-two juvenile yellowfin tuna were distributed among three control tanks maintained at 32‰ and three treatment tanks reduced to 29‰. Three fish were sampled from each control tank at 0 h; three fish were sampled from each low-salinity tank at 6, 24 and 48 h. Gill and liver tissue from the three fish sampled within a tank was pooled to generate one RNA-seq library. Each low-salinity group was compared with the 0 h baseline. (b) Numbers of upregulated and downregulated DEGs in each tissue and comparison.

PCA shows time-associated separation of global expression profiles

Principal component analysis (PCA) separated the gill samples progressively along PC1, from the 0 h baseline toward the 24 and 48 h groups, although one 24 h replicate remained in an intermediate position. In liver, the baseline samples separated mainly along PC2, the 24 h samples occupied a lower-PC2 region, and the 48 h group was more dispersed because one replicate separated strongly along PC1 (Figure 2). These patterns reveal broad temporal differences in transcript abundance while also illustrating variation among biological replicates.

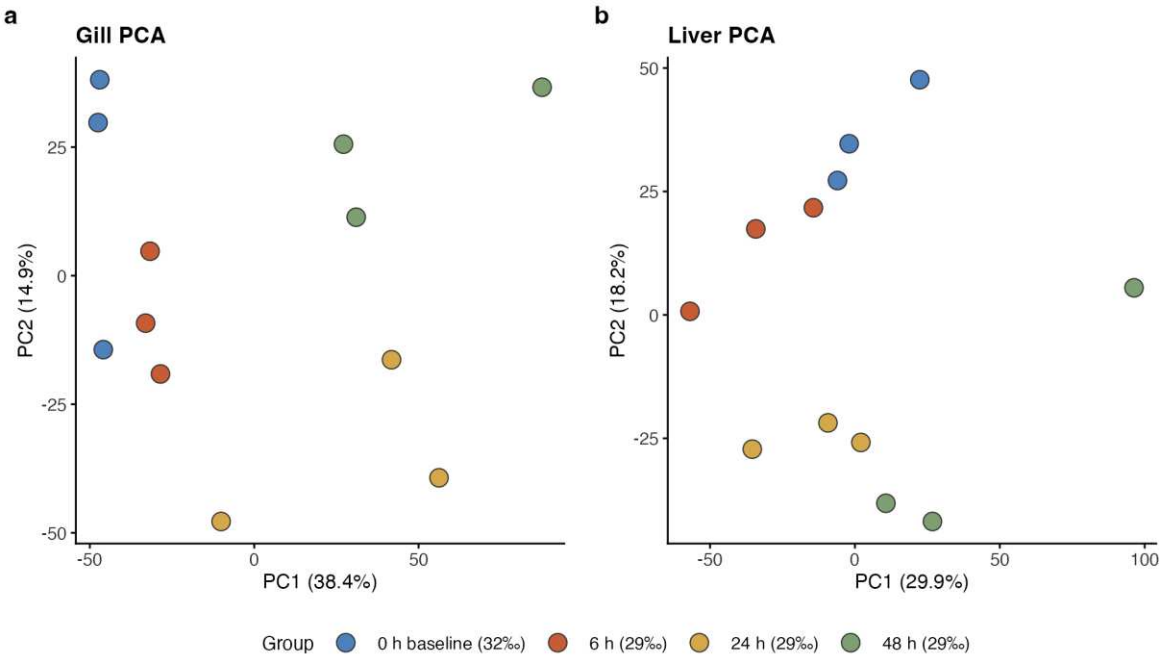

Figure 2. PCA of variance-stabilized counts from all filtered genes in gill (a) and liver (b). Blue, orange, gold and green points identify the 0 h baseline and the 6, 24 and 48 h low-salinity groups, respectively; each point is one independent tank-pool library (n = 3 per group). The axes report the variance explained by each principal component. This unsupervised display shows sample dispersion and time-associated global expression structure; it does not by itself establish treatment effects.

The number of gill DEGs increases over time

After expression filtering, 19,419, 19,183 and 19,066 gill genes were included in the analyses at 6, 24 and 48 h, respectively. Differential expression was detected for 559 genes at 6 h (208 upregulated and 351 downregulated), 2,548 at 24 h (1,669 upregulated and 879 downregulated), and 3,485 at 48 h (1,599 upregulated and 1,886 downregulated) (Table 2). The number of DEGs increased across the three sampling times. Upregulated DEGs predominated at 24 h, whereas downregulated DEGs predominated at 48 h, indicating a change in the direction of branchial expression differences relative to the 0 h baseline.

Figure 3 combines the fold-change and adjusted-P-value distributions with heatmaps of the 30 most statistically supported DEGs at each time point. The heatmaps show gene-standardized expression across biological replicates and illustrate both the direction and consistency of the leading responses.

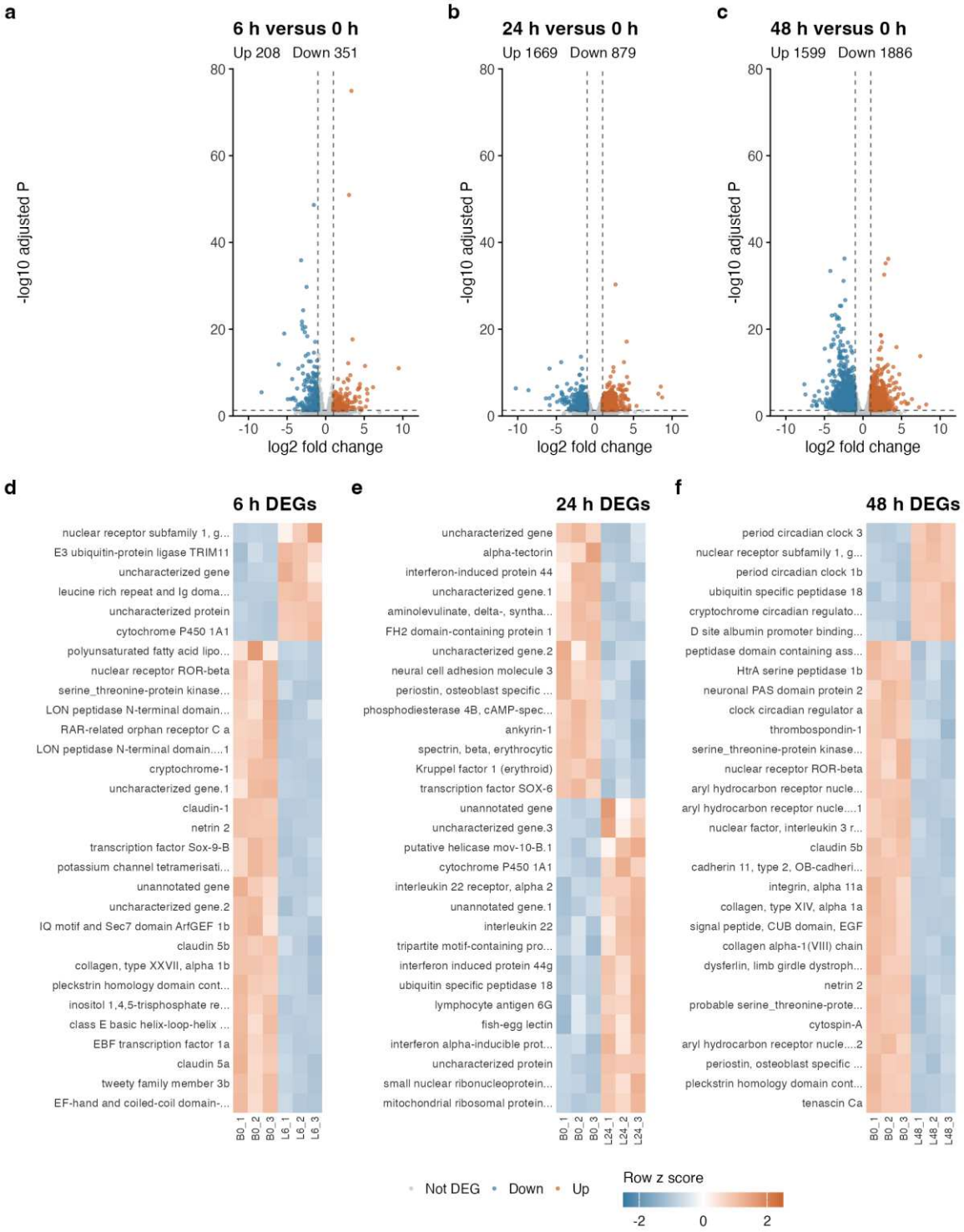

Figure 3. Gill differential expression after 6, 24 and 48 h of low-salinity exposure. (a-c) Volcano plots for 29‰ at each time point relative to the 0 h baseline. Orange and blue points denote upregulated and downregulated DEGs, respectively; grey points do not meet the differential-expression criteria. Dashed lines mark an absolute log2 fold change of 1 and adjusted P = 0.05. (d-f) The 30 DEGs with the smallest adjusted P values in each comparison. Rows are labelled with gene descriptions. Heatmap values are row z scores of variance-stabilized expression. B0, 0 h baseline; L, low salinity. Each group contains three independent tank-level biological replicates.

The number of liver DEGs peaks at 24 h

After expression filtering, 12,643, 12,746 and 12,458 liver genes were included in the analyses at 6, 24 and 48 h, respectively. Differential expression was detected for 333 genes at 6 h (135 upregulated and 198

236 downregulated), 717 at 24 h (360 upregulated and 357 downregulated), and 626 at 48 h (352 upregulated and
237 274 downregulated) (Table 2). Liver had fewer DEGs than gill at each time point, and the largest number of
238 liver DEGs occurred at 24 h. The proportions of upregulated and downregulated genes and the associated
239 functional enrichments also differed among sampling times. Volcano plots and heatmaps of the 30 most
240 statistically supported liver DEGs at each sampling time are shown in Figure 4.

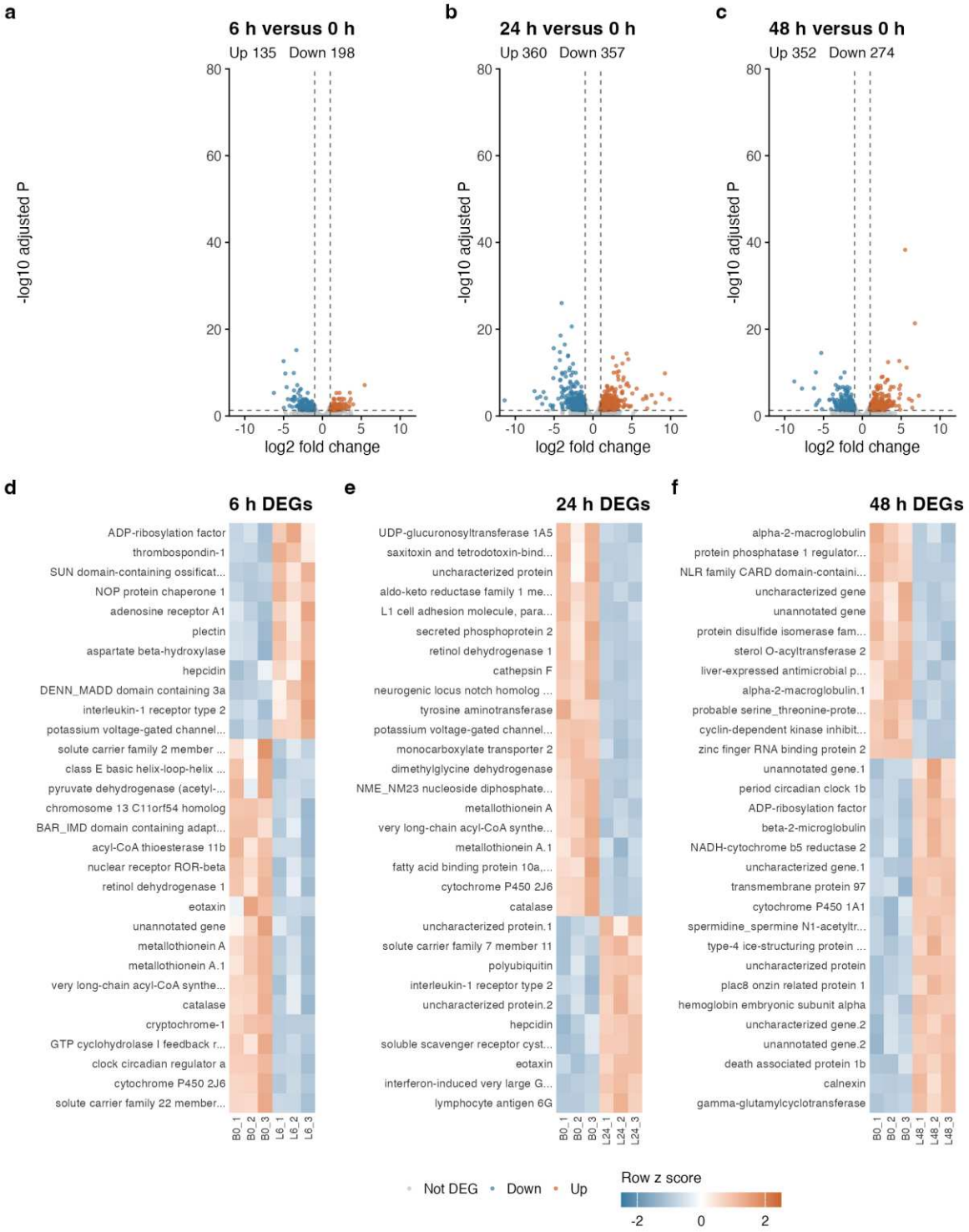

Figure 4. Liver differential expression after 6, 24 and 48 h of low-salinity exposure. Panel organization, colours, statistical criteria and heatmap transformation follow Figure 3. Rows are labelled with gene descriptions. Each 29‰ group was compared with the 32‰ baseline sampled at 0 h. B0, 0 h baseline; L, low salinity.

Most DEGs are detected at a single time point

Across the exposure series, 4,778 gill genes and 1,346 liver genes were differentially expressed at one or more time points. Of these, 140 gill genes and 26 liver genes were differentially expressed in the same direction at 6, 24 and 48 h (Figure 5). The persistent gill response comprised 51 upregulated and 89

downregulated genes, whereas the corresponding liver response comprised 14 upregulated and 12 downregulated genes.

Most DEGs were specific to one sampling point: 195, 1,057 and 1,852 gill genes were detected only at 6, 24 and 48 h, respectively, compared with 168, 429 and 445 liver genes. Thus, a relatively small persistent component was embedded within a larger, temporally changing tissue response.

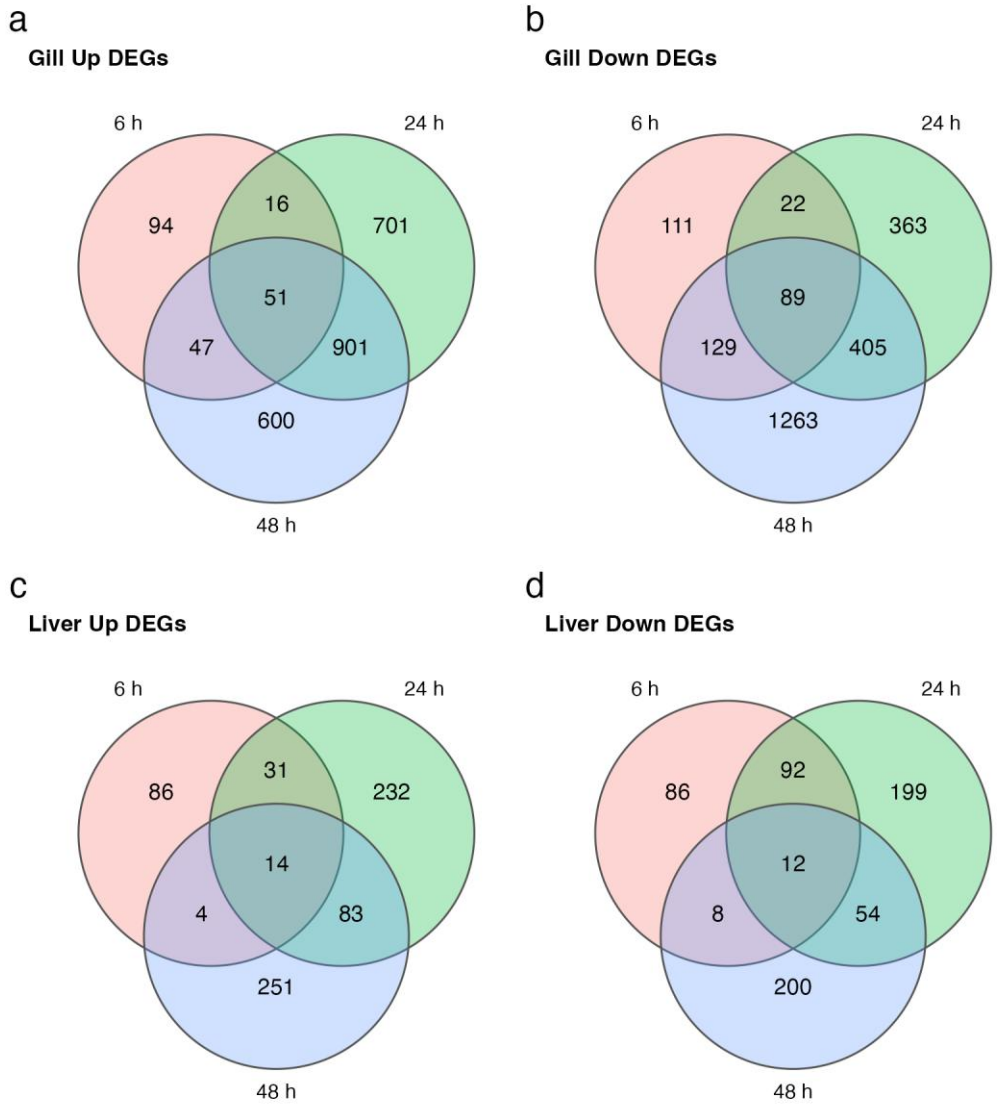

Figure 5. Direction-specific intersections of DEGs identified at 6, 24 and 48 h relative to the 0 h baseline. Upregulated and downregulated genes are shown separately for gill and liver. Counts represent exact gene-set membership; circle areas are schematic. Persistent genes met the differential-expression criteria at all three times and changed in the same direction in every comparison.

Gene set enrichment differs between gill and liver

Gene set enrichment analysis showed strong positive enrichment of oxidative phosphorylation in gill at 6, 24 and 48 h (normalized enrichment score [NES] 3.21, 3.53 and 3.69; BH FDR 2.53×10^{-25}, 7.52×10^{-43} and 1.14×10^{-44}, respectively). Gene sets related to the mitochondrial inner membrane, citrate cycle and protein

263 folding were also positively enriched throughout the exposure. Translation- and ribosome-related gene sets
264 showed particularly strong positive enrichment at 24 and 48 h, with ribosome producing the strongest
265 positive KEGG enrichment at both times. N-glycan biosynthesis remained positively enriched, whereas
266 extracellular-region, cell-adhesion, calcium-signalling and circadian-rhythm gene sets were negatively
267 enriched. Together, these patterns indicate an increasingly prominent transcriptional signature of energy
268 metabolism, protein synthesis and protein homeostasis, accompanied by lower relative expression of several
269 extracellular and signalling gene sets.
270 Liver showed a different temporal pattern. At 6 h, protein processing in the endoplasmic reticulum (NES
271 2.59, BH FDR 8.56×10^{-15}) and N-glycan biosynthesis (NES 2.52, BH FDR 4.02×10^{-7}) were strongly
272 positively enriched, whereas peroxisome, glycine/serine/threonine metabolism, tryptophan metabolism and
273 circadian rhythm were negatively enriched. N-glycan biosynthesis remained positively enriched at 24 h,
274 when proteasome produced the strongest positive KEGG enrichment and several amino-acid- and
275 xenobiotic-metabolism gene sets were negatively enriched. At 48 h, ribosome and oxidative phosphorylation
276 were strongly positively enriched (NES 2.91 and 2.89; BH FDR 8.66×10^{-20} and 5.82×10^{-19}), whereas
277 endoplasmic-reticulum protein processing and fatty-acid degradation were negatively enriched (NES −2.10
278 and −1.95; BH FDR 2.26×10^{-7} and 0.0026). The hepatic expression profile therefore changed from early
279 positive enrichment of protein processing, accompanied by negative enrichment of several amino-acid-
280 metabolism pathways, to strong mitochondrial and translational enrichment at 48 h.
281 Figure 6 summarizes representative GO and KEGG enrichment patterns across all six tissue-by-time
282 comparisons. Filled symbols indicate gene sets that met the Benjamini-Hochberg FDR criterion, whereas
283 open symbols indicate nominal $P < 0.05$.

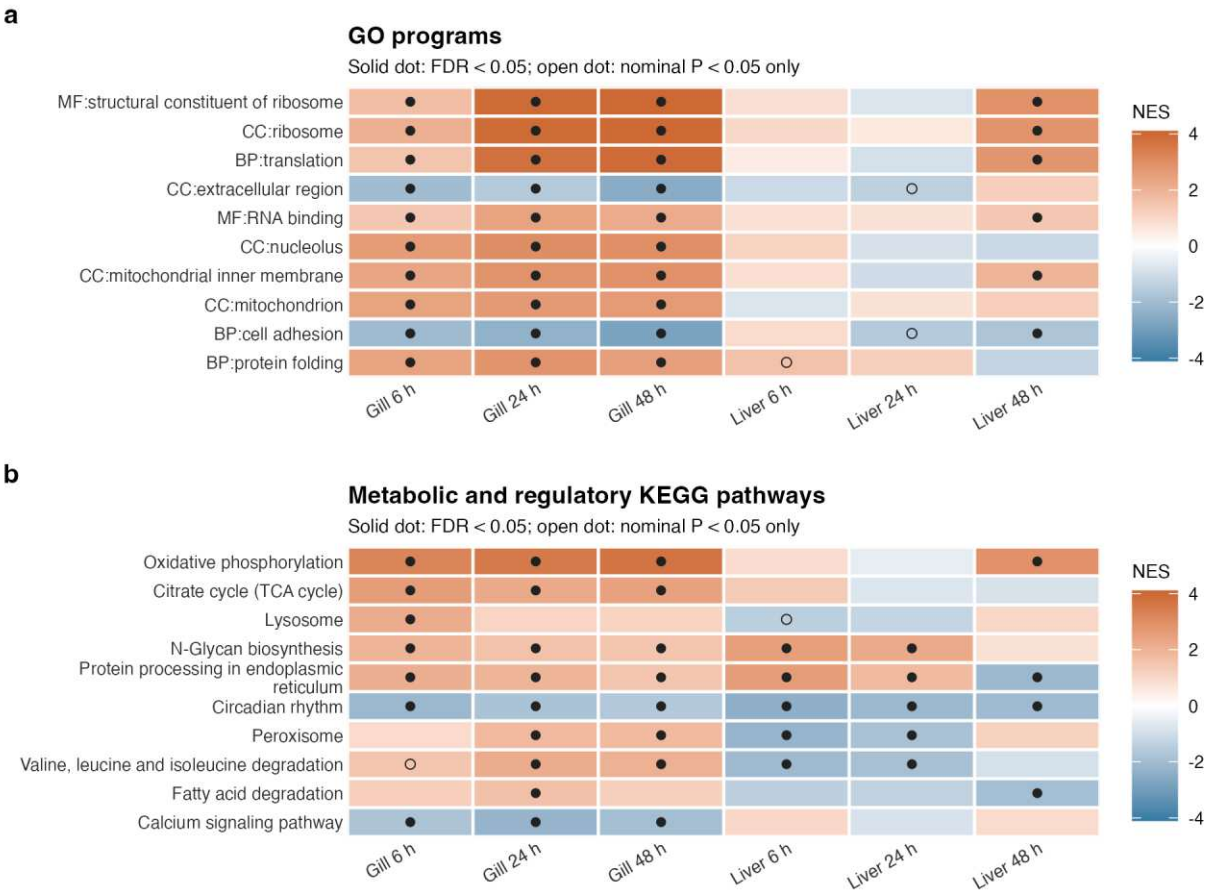

Figure 6. Functional trajectories across the six comparisons with the 0 h baseline. (a) GO and (b) selected KEGG results from preranked GSEA. Tile colour represents the normalized enrichment score (NES); positive values indicate enrichment toward higher Wald statistics in the low-salinity group, and negative values indicate enrichment in the opposite direction. Solid points denote Benjamini-Hochberg FDR < 0.05, open points denote nominal P < 0.05 only, and tiles without points did not reach nominal significance.

Representative enrichment profiles illustrate temporal changes

Running-enrichment profiles were examined for pathways that represented the tissue-specific GSEA patterns (Figure 7). In gill, oxidative-phosphorylation genes accumulated near the positive end of the ranked list at 6, 24 and 48 h, producing NES values of 3.21, 3.53 and 3.69 (BH FDR 2.53×10^{-25}, 7.52×10^{-43} and 1.14×10^{-44}). The broad concentration of pathway members before the enrichment-score maxima shows that this signal was distributed across many mitochondrial genes rather than driven by a single transcript.

The liver profiles reinforced the transition between functional states. N-glycan-biosynthesis genes were concentrated among positive Wald statistics at 6 h (NES 2.52, BH FDR 4.02×10^{-7}), whereas genes assigned to Th1 and Th2 cell differentiation shifted toward the negative end at 24 h (NES −1.64, BH FDR 0.012). This KEGG label denotes conserved signalling components and is not evidence of mammalian lymphocyte differentiation in tuna. By 48 h, liver oxidative-phosphorylation genes were strongly concentrated at the positive end (NES 2.89, BH FDR 5.82×10^{-19}). These profiles support sustained branchial enrichment of

energy-metabolism genes and a hepatic transition from early protein-glycosylation signatures through immune-related changes to later enrichment of mitochondrial gene sets.

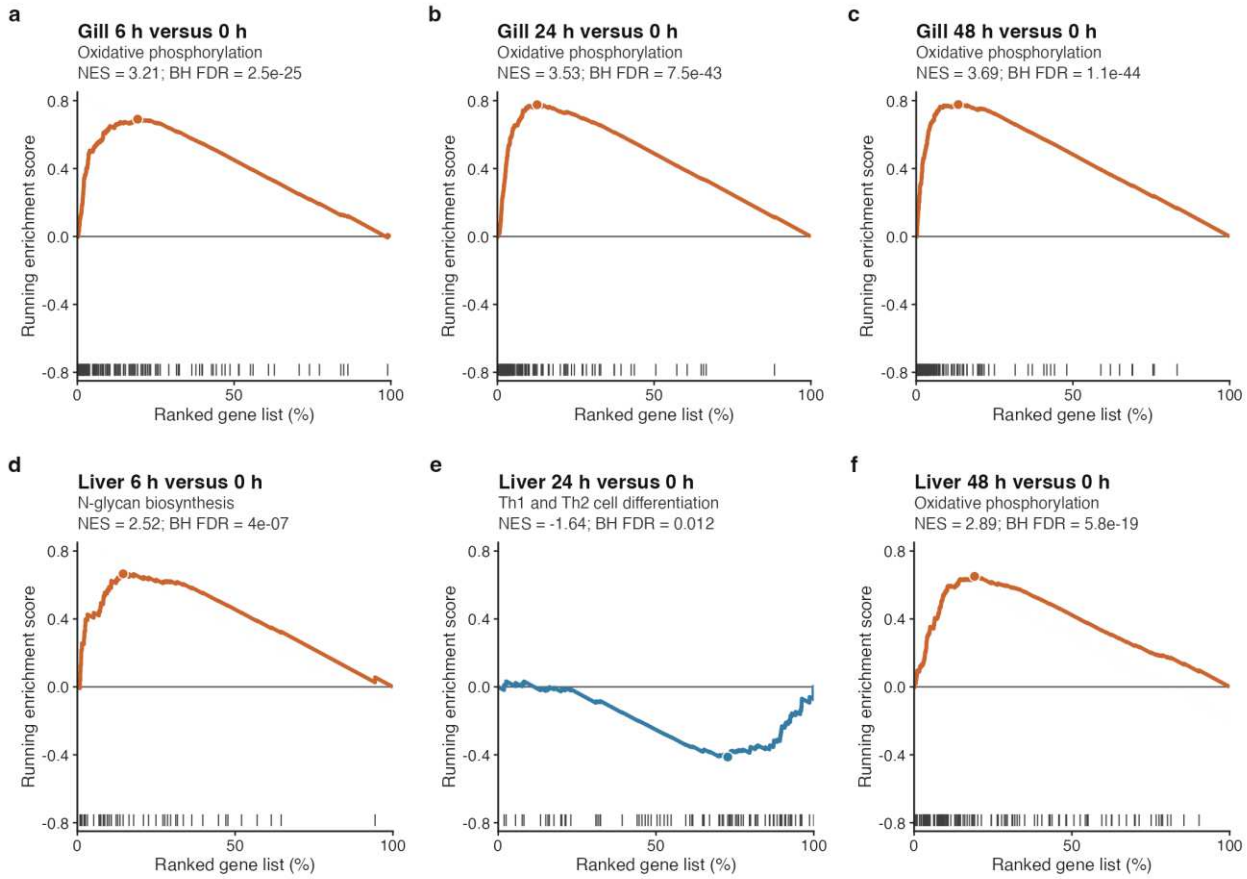

Figure 7. Running-enrichment profiles for representative KEGG pathways. (a-c) Gill oxidative phosphorylation at 6, 24 and 48 h versus 0 h. (d) Liver N-glycan biosynthesis at 6 h, (e) liver Th1 and Th2 cell differentiation at 24 h and (f) liver oxidative phosphorylation at 48 h. Genes were ranked from positive to negative DESeq2 Wald statistics. Orange and blue curves indicate positive and negative normalized enrichment scores (NES), respectively; black ticks show positions of pathway-member genes, and the filled circle marks the maximum absolute running enrichment score. NES and Benjamini-Hochberg FDR are shown in each panel. GSEA used fgseaMultilevel with gene sets of 15-500 mapped genes; Benjamini-Hochberg correction was applied separately to each tissue, time point and gene-set database. Each comparison contained three independent tank-pool libraries per group.

Functional enrichment of persistent and time-specific DEGs

Over-representation analysis identified functional categories associated with persistent and time-specific DEGs. Among the 140 persistent gill DEGs, ECM-receptor interaction and protein digestion and absorption were over-represented, reflecting contributions from extracellular-matrix- and transport-related genes. No GO term or KEGG pathway passed BH correction among the 26 persistent liver DEGs. Gill DEGs specific to 6 h were enriched for circadian rhythm and cell adhesion. The 24 h-specific DEGs were enriched for DNA replication, unfolded-protein binding, proteasome and pyrimidine metabolism, whereas the 48 h-specific DEGs were enriched for extracellular-region, calcium-ion-binding and ECM-receptor-interaction terms.

Among liver DEGs specific to 6 h, oxygen-transporter activity and the haemoglobin complex were strongly over-represented. At 24 h, defense response to bacterium (BH FDR 0.0041), defense response to virus (BH FDR 0.040) and pyrimidine metabolism (BH FDR 0.015) were over-represented. The 48 h-specific DEGs were enriched for extracellular-region and circadian-rhythm terms. Figure 8 distinguishes results supported at BH FDR < 0.05 from exploratory terms with BH FDR between 0.05 and 0.10.

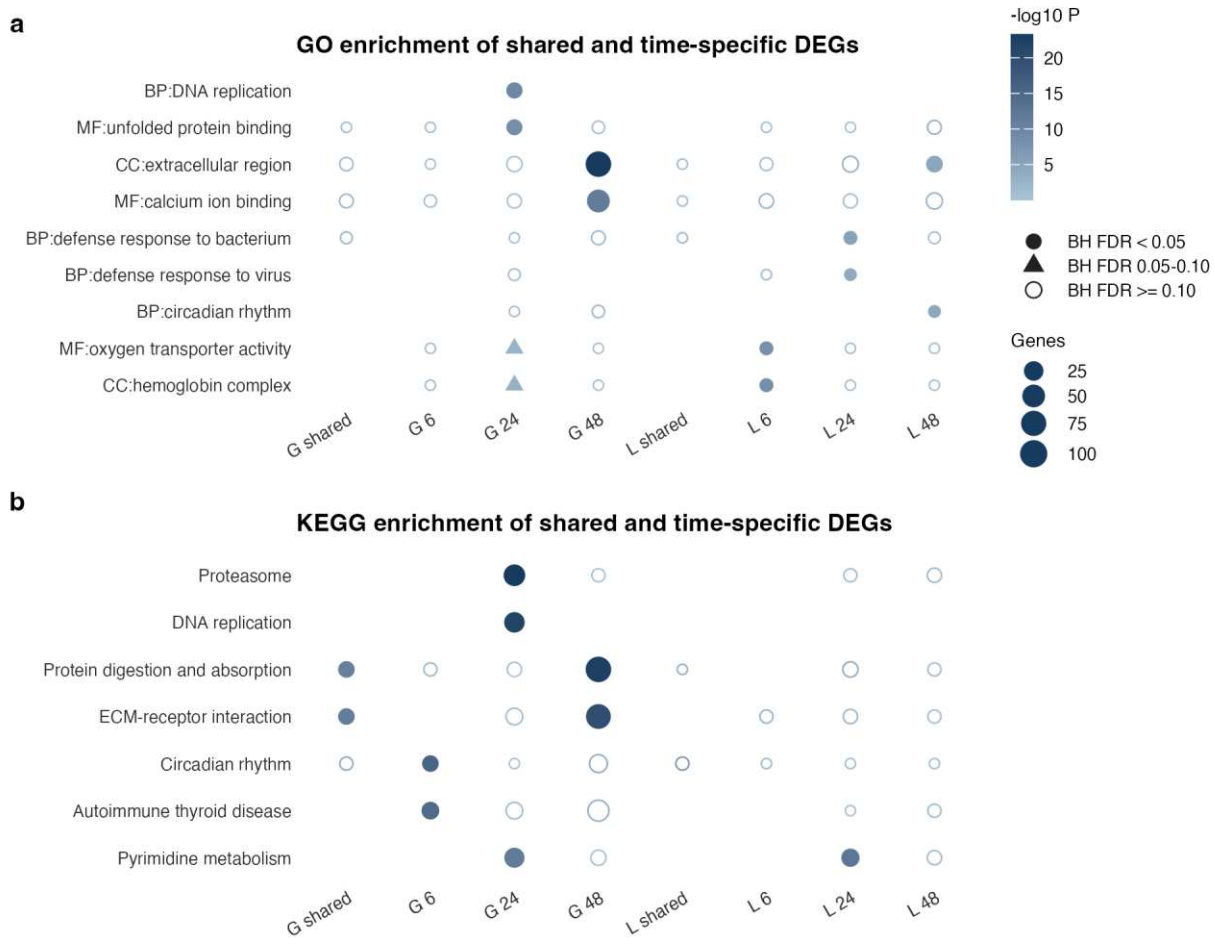

Figure 8. Over-representation analysis of persistent and time-specific DEG sets. Within each database and gene set, up to two terms with BH FDR < 0.05 and at least three overlapping DEGs were selected. If none met these criteria, up to two terms with BH FDR < 0.10 and at least three overlapping DEGs were selected. The union of selected terms is displayed across all gene sets. Filled circles, triangles and open circles indicate BH FDR < 0.05, 0.05 ≤ BH FDR < 0.10 and BH FDR ≥ 0.10, respectively. Point area indicates the number of overlapping DEGs and colour indicates the nominal P value. G and L denote gill and liver; shared denotes persistent DEGs, and 6, 24 and 48 denote DEGs detected only at the indicated time. This analysis complements the ranked enrichment results in Figures 6 and 7.

Metabolic and immune-related gene sets change concurrently

In gill, sustained positive enrichment of mitochondrial, translational and protein-folding gene sets occurred alongside negative enrichment of B-cell-receptor signalling, phagocytosis, leukocyte migration and cytokine-receptor interactions at 24 or 48 h. At 24 h, liver DEGs were enriched for bacterial- and viral-defence terms, whereas the Th1/Th2 differentiation gene set was negatively enriched. At 48 h, oxidative phosphorylation

and translation were strongly positively enriched, accompanied by nominal positive trends in cytokine-related gene sets. KEGG pathways named after human diseases were interpreted according to their conserved mitochondrial or immune-signalling genes and do not indicate the presence of those diseases in tuna. These results show concurrent changes in metabolic and immune-related gene sets in both tissues during low-salinity exposure [10,11,14,15].

Gene-level expression patterns are consistent with pathway-level enrichment

Figure 9 shows log2 fold changes for representative genes in selected KEGG pathways. In gill, genes associated with oxidative phosphorylation had predominantly positive log2 fold changes at 24 and 48 h, whereas calcium-signalling genes, including *avpr1aa*, and circadian-clock genes had predominantly negative values. Liver genes assigned to the selected pathways varied more in direction across sampling times, consistent with the temporal changes observed in gene-set enrichment.

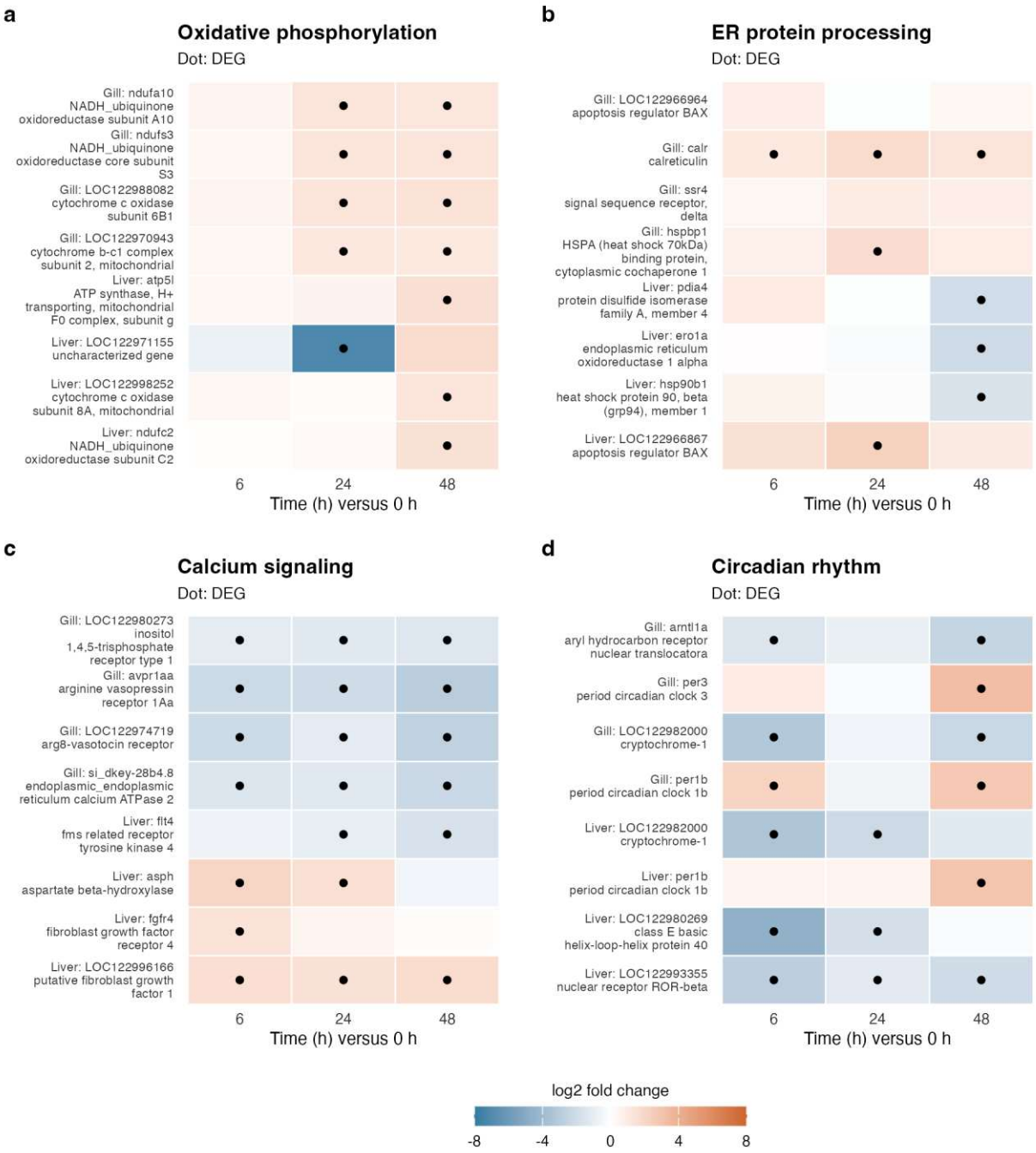

Figure 9. Gene-level expression patterns in selected KEGG pathways. Each tile shows the DESeq2 log2 fold change for 29‰ at 6, 24 or 48 h relative to 0 h. Rows show gene symbols or identifiers together with concise functional descriptions, grouped by pathway and tissue. Solid black points identify DEGs.

Co-expression among persistent differentially expressed genes

Co-expression networks were constructed from the 12 variance-stabilized samples per tissue to describe covariation among genes that were differentially expressed in the same direction at all three sampling times (Figure 10). For each tissue, the five upregulated and five downregulated genes with the highest degree in the complete network were displayed. The gill subnetwork contained 43 edges, including 18 positive and 25 negative correlations, whereas the liver subnetwork contained 21 edges, including 12 positive and nine

negative correlations. Highly connected gill genes included coiled-coil domain-containing protein 3b, chondroitin sulfate proteoglycan 4, ubiquitin-specific peptidase 18, annexin A14 and a mitochondrial outer-membrane channel. In liver, the displayed correlations involved genes associated with retinol and one-carbon metabolism, reticulocalbin 3, a creatine transporter, sorting nexin 16 and other persistent DEGs. These correlations describe expression covariation and do not imply regulatory interactions.

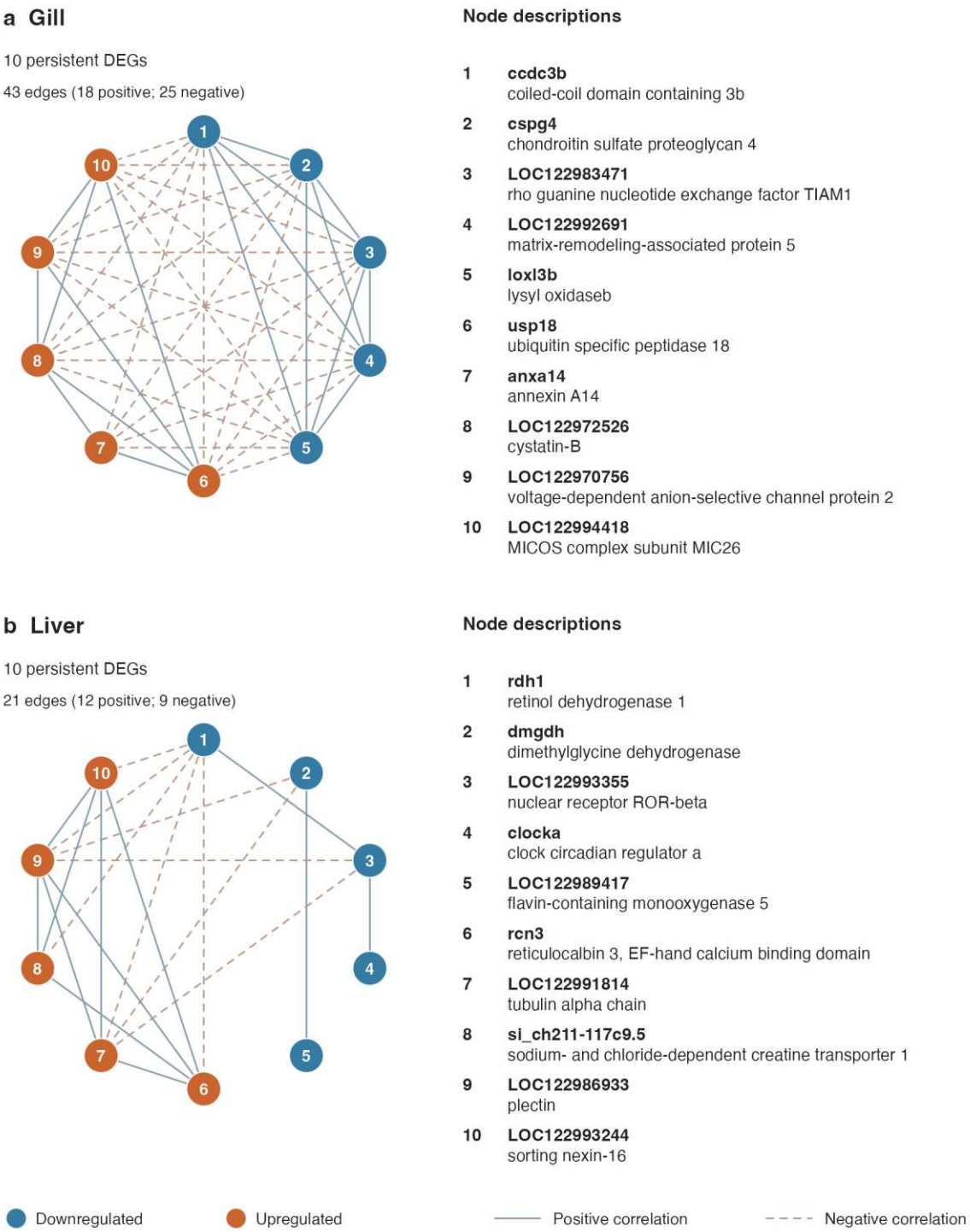

Figure 10. Co-expression networks of persistent DEGs in gill (a) and liver (b). Each panel displays the five upregulated and five downregulated genes ranked highest by degree in the full tissue network. Numbers map nodes to the adjacent gene descriptions. Edges indicate absolute Spearman correlation ≥ 0.80 across 12 variance-stabilized samples per tissue; solid and dashed lines indicate positive and negative correlations. Node colour indicates the consistent direction of change relative to 0 h. Circular positions and equal node sizes are for display only. Correlations are descriptive and do not establish regulatory interactions.

qRT-PCR comparison of selected expression profiles

The relative expression profiles of eight selected genes were compared with RNA-seq after normalization to a 0 h baseline of 1 (Figures S4 and S5). In gill, *atp5l*, *sod1* and *apoeb* increased across the exposure series, whereas *blmh* and *b2m* peaked at 24 h and declined at 48 h. *hspa8b* showed an early increase at 6 h followed by a decline, *usp18* remained elevated at 24 and 48 h, and *dmgdh* remained below the baseline throughout exposure. These temporal patterns were broadly consistent between the two methods, although the fold-change magnitudes differed (Figure S4).

In liver, *atp5l* and *b2m* showed their highest expression at 48 h, while *hspa8b*, *apoeb* and *usp18* peaked at 24 h. *dmgdh* remained below the baseline at all exposure times. The two methods generally captured similar temporal patterns, with gene-specific differences. For example, hepatic *blmh* expression measured by qRT-PCR rebounded above the baseline at 48 h, whereas its RNA-seq value remained below the baseline (Figure S5). The comparison therefore supports broad agreement in expression trends without implying identical fold changes or statistical significance.

Discussion

The principal finding is that gill and liver followed different transcriptional trajectories during the same low-salinity exposure. Gill retained a mitochondrial and protein-homeostasis signature as the number of DEGs increased, whereas liver shifted from early protein processing to immune-related changes and later mitochondrial and translational enrichment. Combining ranked enrichment with temporal intersections shows that sustained functional themes can coexist with substantial changes in the genes meeting differential-expression criteria. This distinction is important for interpreting salinity-responsive transcriptomes: a persistent pathway signature need not involve an identical set of significant genes at every sampling time.

The sustained positive enrichment of branchial oxidative phosphorylation and the citrate cycle is consistent with increased energetic demands at the environmental interface. Gill ion transport, acid-base regulation, gas exchange and nitrogen excretion require ATP, and mitochondrion-rich cells alter their transport machinery during salinity acclimation [2,3,37-40]. ATP synthase, respiratory-chain and tricarboxylic-acid-cycle genes contributed broadly to the ranked enrichment, which strengthened from 6 to 48 h. Related changes in branchial energy-metabolism genes have been reported in tilapia, Asian seabass, killifish and other teleosts

exposed to altered salinity [6,19,20,41-46]. The present results therefore indicate a progressively stronger mitochondrial transcriptional response in yellowfin tuna gill.

The mitochondrial signature was accompanied by positive enrichment of protein synthesis and protein quality-control processes. Ribosome, translation, nucleolar, protein-folding and proteasome gene sets became especially prominent at 24 and 48 h, while N-glycan biosynthesis remained positively enriched. Protein synthesis, folding, glycosylation, trafficking and degradation act together to maintain membrane and secreted proteins [47-51]. In gill, these processes may support turnover of ion transporters, channels, receptors and junctional proteins during adjustment of the branchial epithelium [7,8,52,53]. Enrichment of DNA replication and unfolded-protein binding among 24 h-specific DEGs further suggests increased cellular renewal and proteostatic demand, while the extracellular and calcium-binding terms at 48 h indicate continued change at the tissue interface.

The gill response was selective rather than uniformly positive. Extracellular-region, cell-adhesion and calcium-signalling gene sets were negatively enriched across much of the exposure series. B-cell-receptor signalling, Fc-receptor-mediated phagocytosis, leukocyte migration and cytokine-receptor interactions were also negatively enriched at 24 or 48 h. These pathway names represent conserved signalling modules and do not directly measure particular leukocyte populations. Nevertheless, their coordinated negative enrichment indicates that the strong metabolic and protein-homeostasis response coincided with altered expression of mucosal immune functions. This relationship is biologically relevant because the gill is both an osmoregulatory epithelium and an immune surface [14-17,52,54].

Liver showed an earlier emphasis on protein processing. Positive enrichment of endoplasmic-reticulum protein processing and N-glycan biosynthesis at 6 h indicates increased expression of genes involved in protein folding, modification and export. In parallel, peroxisomal and several amino-acid-degradation pathways were negatively enriched, and 6 h-specific DEGs were enriched for oxygen-transport and haemoglobin terms. These findings indicate rapid reorganization of hepatic protein and substrate metabolism rather than a uniform increase in hepatic activity. Because the liver integrates carbohydrate, amino-acid and lipid metabolism with production of circulating proteins, it is well positioned to redistribute metabolic resources during osmotic adjustment [10-13,23,45,55,56].

At 24 h, hepatic metabolic changes coincided with immune-related transcription. Defence responses to bacteria and viruses, innate immune response, lysozyme activity and cytolysis were over-represented among

DEGs, whereas Th1/Th2 differentiation and leukocyte-migration gene sets were negatively enriched. Together, these analyses identify changes in multiple immune-related functions. Teleost liver contributes complement proteins, antimicrobial molecules, iron regulation and acute-phase responses [15,54,57,58]. Comparable coupling between hepatic metabolism and immunity has been observed during salinity acclimation in spotted sea bass, marine medaka, yellowfin seabream and other fishes [12,17,23]. In yellowfin tuna, the strongest hepatic immune-related pattern therefore coincided with the 24 h peak in DEG number. By 48 h, the hepatic profile was dominated by positive enrichment of oxidative phosphorylation and ribosome gene sets, whereas endoplasmic-reticulum protein processing and fatty-acid degradation were negatively enriched. The change from positive ER-processing enrichment at 6 h to negative enrichment at 48 h, together with lower fatty-acid-catabolic scores, indicates a shift in the transcriptional programs associated with hepatic fuel use and protein handling. Salinity acclimation can alter circulating fuels, hepatic lipid metabolism and the balance among carbohydrate, amino-acid and fatty-acid utilization [10-13,59]. Transcript abundance does not measure metabolic flux, however, so these data support a change in the hepatic metabolic state without establishing the amount of ATP produced or lipid oxidized.

Temporal intersections separated a persistent gene component from responses detected at individual sampling times. The 140 persistent gill genes and 26 persistent liver genes provide candidates for studying sustained responses, while time-specific sets emphasized branchial proteostasis and extracellular functions and hepatic oxygen transport and immune defence. The persistent gill set was enriched for extracellular-matrix-related categories; the smaller liver set yielded no FDR-supported term. These differences complement the ranked enrichment results, which describe broader pathway shifts without requiring every contributing gene to exceed the DEG threshold. A gene classified as time-specific may show a weaker response at another time, so this classification refers to statistical detection rather than exclusive biological activity. The 10-node networks summarize covariation within the persistent sets and can help prioritize combinations of candidates for follow-up. With only 12 samples per tissue, they do not establish regulatory relationships [60].

Circadian-rhythm signals were negative in both organs and were present in persistent or time-specific analyses. Peripheral fish clocks integrate light, feeding, endocrine and metabolic information [61-65]. Their coordinated shift may therefore reflect part of the organism-wide adjustment that accompanies altered energy use. Calcium signalling in gill showed a similarly consistent negative pattern. These regulatory signals could

influence transport, secretion and immune-cell communication, but their physiological meaning requires targeted sampling across the daily cycle and direct measurement of downstream activity.

The comparative transcriptomic evidence extends earlier observations of tissue-specific antioxidant and digestive responses under the same salinity transition [25,26]. It also places yellowfin tuna alongside teleost studies reporting branchial transport and metabolic responses and hepatic changes in substrate metabolism and defence [10,12,17,22,23]. The contribution here is the resolution of these themes across two organs and successive exposure stages, revealing sustained branchial pathway enrichment alongside a changing hepatic profile. The resulting gene sets can guide functional studies beyond the selected qRT-PCR targets. Pairing branchial transporter localization and Na^+/K^+-ATPase activity with respiratory measurements would test the physiological meaning of the mitochondrial signature [44,53]. In liver, integrating transcript profiles with protein abundance, metabolites and immune-function measurements would test whether the observed shifts in metabolic and immune-related gene sets translate into coordinated functional changes.

Several limitations define the scope of these conclusions. All low-salinity groups were compared with the same 32‰ baseline collected at 0 h, based on the assumption that RNA abundance remains stable in normal seawater. Because the experiment did not include 32‰ RNA-seq controls at 6, 24 and 48 h, it cannot estimate a salinity-by-time interaction or separate exposure-associated changes from ordinary temporal variation. Three pooled tank replicates per group limit precision, and pooling obscures fish-to-fish variation. The pathway analyses describe coordinated transcript abundance rather than protein activity, cell composition or physiological flux, and the co-expression networks are exploratory. A factorial salinity-by-time experiment with independent tanks, a recovery phase and integrated physiological measurements would directly test the proposed model [60,66-68].

Conclusions

Comparative profiling of gill and liver identified distinct temporal patterns of gene expression during acute low-salinity exposure in juvenile yellowfin tuna. Gill showed sustained enrichment of mitochondrial energy metabolism and protein homeostasis, together with stronger translation-related enrichment and negative enrichment of several immune-related gene sets at later times. Liver progressed from early protein processing and glycosylation to selective immune-related changes at 24 h and mitochondrial and translational enrichment at 48 h. Negative enrichment of hepatic fatty-acid degradation and endoplasmic-

reticulum protein processing further distinguished the later response. Persistent DEG sets coexisted with substantial differences among sampling times, showing why both organ identity and exposure stage are needed to interpret the transcriptomic profile.

These findings provide a molecular framework for investigating salinity-associated metabolic and immune responses in a pelagic marine fish. The persistent genes, stage-associated gene sets and contrasting pathway trajectories identify candidates and sampling windows for targeted experiments. Their value extends beyond the eight qRT-PCR targets to the broader transcriptional programs resolved by the analysis. Linking these programs to protein activity, metabolite turnover, epithelial transport and immune function will establish their physiological consequences. Such comparisons will clarify which responses are shared across teleosts and which depend on the organ, species or salinity regime.

Abbreviations

DEG, differentially expressed gene; ER, endoplasmic reticulum; FDR, false discovery rate; GO, Gene Ontology; GSEA, gene set enrichment analysis; KEGG, Kyoto Encyclopedia of Genes and Genomes; NES, normalized enrichment score; ORA, over-representation analysis; PCA, principal component analysis; qRT-PCR, quantitative real-time polymerase chain reaction; RNA-seq, RNA sequencing.

Declarations

Ethics approval and consent to participate

No collection permit was required for these specimens. All animal handling, salinity exposure and tissue sampling were performed in accordance with the protocol approved by the Animal Care and Use Committee of the South China Sea Fisheries Research Institute, Chinese Academy of Fishery Sciences (BIOL5346, 9 May 2022).

Consent for publication

Not applicable.

Availability of data and materials

The raw RNA-seq reads generated in this study have been deposited in the NCBI Sequence Read Archive (SRA) under BioProject accession PRJNA1537459. Sequencing-quality metrics and supplementary figures, including the qRT-PCR comparisons, are provided in the supplementary information.

Competing interests

The authors declare that they have no competing interests.

Funding

This work was supported by the 2025 Research on breeding technology of candidate species for Guangdong modern marine ranching (2025-MRB-00-001); the Central Public interest Scientific Institution Basal Research Fund, CAFS (2025XT03, 2023TD58, 2026TS01); the National Natural Science Foundation of China (32460927); the Science and Technology Special Fund of Hainan Province (ZDYF2024XDNY247); and the Guangdong Province Overseas Distinguished Scholars Program (MS202500183).

Authors' contributions

Conceptualization, Ziyi Jiang and Zhengyi Fu; methodology, Ziyi Jiang; software, Ziyi Jiang and Junhua Huang; validation, Junhua Huang; formal analysis, Ziyi Jiang; investigation, Ziyi Jiang; resources, Zhenhua Ma and Rui Yang; data curation, Ziyi Jiang; writing (original draft preparation), Ziyi Jiang; writing (review and editing), Zhenhua Ma, Dianchang Zhang and Xuxiong Huang; supervision, Zhenhua Ma and Dianchang Zhang; project administration, Jing Hu and Rui Yang; funding acquisition, Zhenhua Ma, Rui Yang and Zhiyong Jiang. All authors have read and approved the final manuscript.

Acknowledgements

The authors thank the staff of the Lingshui Research Station for animal husbandry and sampling support.

Use of AI tools

OpenAI Codex (OpenAI) was used to assist with code development.

References

1. Durack PJ, Wijffels SE, Matear RJ. Ocean salinities reveal strong global water cycle intensification during 1950 to 2000. Science. 2012;336:455-458. doi:10.1126/science.1212222.

2. Evans DH, Piermarini PM, Choe KP. The multifunctional fish gill: dominant site of gas exchange, osmoregulation, acid base regulation, and excretion of nitrogenous waste. Physiol Rev. 2005;85:97-177. doi:10.1152/physrev.00050.2003.

3. Hwang PP, Lee TH. New insights into fish ion regulation and mitochondrion rich cells. Comp Biochem Physiol A Mol Integr Physiol. 2007;148:479-497. doi:10.1016/j.cbpa.2007.06.416.

4. Kultz D. Physiological mechanisms used by fish to cope with salinity stress. J Exp Biol. 2015;218:1907-1914. doi:10.1242/jeb.118695.

5. Schulte PM. What is environmental stress? Insights from fish living in a variable environment. J Exp Biol. 2014;217:23-34. doi:10.1242/jeb.089722.

6. Zikos A, Seale AP, Lerner DT, Grau EG, Korsmeyer KE. Effects of salinity on metabolic rate and branchial expression of genes involved in ion transport and metabolism in Mozambique tilapia (Oreochromis mossambicus). Comp Biochem Physiol A Mol Integr Physiol. 2014;178:121-131. doi:10.1016/j.cbpa.2014.08.016.

7. Tang CH, Lee TH. Early response of protein quality control in gills is associated with survival of hypertonic shock in Mozambique tilapia. PLoS One. 2013;8:e63112. doi:10.1371/journal.pone.0063112.

8. Umam K, Chuang HJ, Chiu L, Yang WK, Wang YC, Wu WY, Lee TH. Potential osmoprotective roles of branchial heat shock proteins towards Na+, K+-ATPase in milkfish (Chanos chanos) exposed to hypotonic stress. Comp Biochem Physiol A Mol Integr Physiol. 2020;248:110749. doi:10.1016/j.cbpa.2020.110749.

9. Boeuf G, Payan P. How should salinity influence fish growth? Comp Biochem Physiol C Toxicol Pharmacol. 2001;130:411-423. doi:10.1016/S1532-0456(01)00268-X.

10. Si Y, Wen H, Li Y, et al. Liver transcriptome analysis reveals extensive transcriptional plasticity during acclimation to low salinity in Cynoglossus semilaevis. BMC Genomics. 2018;19:464. doi:10.1186/s12864-018-4825-4.

11. Chen J, Cai B, Tian C, et al. RNA sequencing analysis reveals liver lipid metabolism divergent adaptive response to low- and high-salinity stress in spotted scat (Scatophagus argus). Animals. 2023;13:1503. doi:10.3390/ani13091503.

12. Zhang X, Wen H, Wang H, Ren Y, Zhao J, Li Y. RNA-Seq analysis of salinity stress-responsive transcriptome in the liver of spotted sea bass (Lateolabrax maculatus). PLoS One. 2017;12:e0173238. doi:10.1371/journal.pone.0173238.

13. Sangiao-Alvarellos S, Arjona FJ, Martin del Rio MP, Miguez JM, Mancera JM, Soengas JL. Time course of osmoregulatory and metabolic changes during osmotic acclimation in Sparus auratus. J Exp Biol. 2005;208:4291-4304. doi:10.1242/jeb.01900.

14. Li J, Xue L, Cao M, et al. Gill transcriptomes reveal expression changes of genes related with immune and ion transport under salinity stress in silvery pomfret (Pampus argenteus). Fish Physiol Biochem. 2020;46:1255-1277. doi:10.1007/s10695-020-00786-9.

15. Magnadóttir B. Innate immunity of fish (overview). Fish Shellfish Immunol. 2006;20:137-151. doi:10.1016/j.fsi.2004.09.006.

16. Gu J, Dai S, Liu H, Cao Q, Yin S, Lai KP, Tse WKF, Wong CKC, Shi H. Identification of immune-related genes in gill cells of Japanese eels (Anguilla japonica) in adaptation to water salinity changes. Fish Shellfish Immunol. 2018;73:288-296. doi:10.1016/j.fsi.2017.12.026.

17. Lin G, Zheng M, Gao D, Li S, Fang W, Huang J, et al. Hypoosmotic stress induced tissue-specific immune responses of yellowfin seabream (Acanthopagrus latus) revealed by transcriptomic analysis. Fish Shellfish Immunol. 2020;99:473-482. doi:10.1016/j.fsi.2020.02.028.

18. Wang D, Liu N, Kong X, Zhu X, Wang Y, Hu J, et al. Single-cell transcriptomic dynamics of scallop heart reveals the heterogeneous response to heat stress. BMC Biol. 2025;23:98. doi:10.1186/s12915-025-02210-1.

19. Evans TG, Somero GN. A microarray-based transcriptomic time-course of hyper- and hypo-osmotic stress signaling events in the euryhaline fish Gillichthys mirabilis: osmosensors to effectors. J Exp Biol. 2008;211:3636-3649. doi:10.1242/jeb.022160.

20. Whitehead A, Roach JL, Zhang S, Galvez F. Salinity- and population-dependent genome regulatory response during osmotic acclimation in the killifish (Fundulus heteroclitus) gill. J Exp Biol. 2012;215:1293-1305. doi:10.1242/jeb.062075.

21. Whitehead A, Roach JL, Zhang S, Galvez F. Genomic mechanisms of evolved physiological plasticity in killifish distributed along an environmental salinity gradient. Proc Natl Acad Sci U S A. 2011;108:6193-6198. doi:10.1073/pnas.1017542108.

22. Martos-Sitcha JA, Mancera JM, Calduch-Giner JA, Yúfera M, Martínez-Rodríguez G, Pérez-Sánchez J. Unraveling the tissue-specific gene signatures of gilthead sea bream after hyper- and hypo-osmotic challenges. PLoS One. 2016;11:e0148113. doi:10.1371/journal.pone.0148113.

23. Liang P, Saqib HSA, Lin Z, Zheng R, Qiu Y, Xie Y, et al. RNA-seq analyses of marine medaka (Oryzias melastigma) reveals salinity responsive transcriptomes in the gills and livers. Aquat Toxicol. 2021;240:105970. doi:10.1016/j.aquatox.2021.105970.

598 24. Dewar H, Graham JB. Studies of tropical tuna swimming performance in a large water tunnel: I.
599 Energetics. J Exp Biol. 1994;192:13-31. doi:10.1242/jeb.192.1.13.
600 25. Zhang N, Yang R, Fu Z, Yu G, Ma Z. Mechanisms of digestive enzyme response to acute salinity stress
601 in juvenile yellowfin tuna (*Thunnus albacares*). Animals. 2023;13:3454. doi:10.3390/ani13223454.
602 26. Zhou S, Zhang N, Fu Z, Yu G, Ma Z, Zhao L. Impact of salinity changes on the antioxidation of juvenile
603 yellowfin tuna (*Thunnus albacares*). J Mar Sci Eng. 2023;11:132. doi:10.3390/jmse11010132.
604 27. Livak KJ, Schmittgen TD. Analysis of relative gene expression data using real-time quantitative PCR
605 and the $2^{-\Delta\Delta CT}$ method. Methods. 2001;25:402-408. doi:10.1006/meth.2001.1262.
606 28. Bolger AM, Lohse M, Usadel B. Trimmomatic: a flexible trimmer for Illumina sequence data.
607 Bioinformatics. 2014;30:2114-2120. doi:10.1093/bioinformatics/btu170.
608 29. Kim D, Paggi JM, Park C, Bennett C, Salzberg SL. Graph-based genome alignment and genotyping with
609 HISAT2 and HISAT-genotype. Nat Biotechnol. 2019;37:907-915. doi:10.1038/s41587-019-0201-4.
610 30. Pertea M, Pertea GM, Antonescu CM, Chang TC, Mendell JT, Salzberg SL. StringTie enables improved
611 reconstruction of a transcriptome from RNA-seq reads. Nat Biotechnol. 2015;33:290-295.
612 doi:10.1038/nbt.3122.
613 31. Love MI, Huber W, Anders S. Moderated estimation of fold change and dispersion for RNA-seq data
614 with DESeq2. Genome Biol. 2014;15:550. doi:10.1186/s13059-014-0550-8.
615 32. Benjamini Y, Hochberg Y. Controlling the false discovery rate: a practical and powerful approach to
616 multiple testing. J R Stat Soc Series B Stat Methodol. 1995;57:289-300. doi:10.1111/j.2517-
617 6161.1995.tb02031.x.
618 33. Ashburner M, Ball CA, Blake JA, et al. Gene Ontology: tool for the unification of biology. Nat Genet.
619 2000;25:25-29. doi:10.1038/75556.
620 34. Kanehisa M, Sato Y, Kawashima M. KEGG for taxonomy-based analysis of pathways and genomes.
621 Nucleic Acids Res. 2023;51:D587-D592. doi:10.1093/nar/gkac963.
622 35. Subramanian A, Tamayo P, Mootha VK, et al. Gene set enrichment analysis: a knowledge-based
623 approach for interpreting genome-wide expression profiles. Proc Natl Acad Sci U S A. 2005;102:15545-
624 15550. doi:10.1073/pnas.0506580102.
625 36. Korotkevich G, Sukhov V, Budin N, Shpak B, Artyomov MN, Sergushichev A. Fast gene set enrichment
626 analysis. bioRxiv. 2016:060012. doi:10.1101/060012.

627 37. Fiol DF, Kültz D. Osmotic stress sensing and signaling in fishes. FEBS J. 2007;274:5790-5798.
628 doi:10.1111/j.1742-4658.2007.06099.x.
629 38. Evans TG. Co-ordination of osmotic stress responses through osmosensing and signal transduction
630 events in fishes. J Fish Biol. 2010;76:1903-1925. doi:10.1111/j.1095-8649.2010.02590.x.
631 39. Sakamoto T, Uchida K, Yokota S. Regulation of the ion-transporting mitochondrion-rich cell during
632 adaptation of teleost fishes to different salinities. Zool Sci. 2001;18:1163-1174. doi:10.2108/zsj.18.1163.
633 40. Tseng YC, Hwang PP. Some insights into energy metabolism for osmoregulation in fish. Comp Biochem
634 Physiol C Toxicol Pharmacol. 2008;148:419-429. doi:10.1016/j.cbpc.2008.04.009.
635 41. Ern R, Huong DTT, Cong NV, Bayley M, Wang T. Effect of salinity on oxygen consumption in fishes: a
636 review. J Fish Biol. 2014;84:1210-1220. doi:10.1111/jfb.12330.
637 42. Vij S, Purushothaman K, Sridatta PSR, et al. Transcriptomic analysis of gill and kidney from Asian
638 seabass (Lates calcarifer) acclimated to different salinities reveals pathways involved with euryhalinity.
639 Genes. 2020;11:733. doi:10.3390/genes11070733.
640 43. Root L, Campo A, MacNiven L, Con P, Cnaani A, Kultz D. Nonlinear effects of environmental salinity
641 on the gill transcriptome versus proteome of Oreochromis niloticus modulate epithelial cell turnover.
642 Genomics. 2021;113:3235-3249. doi:10.1016/j.ygeno.2021.07.016.
643 44. Scott GR, Richards JG, Forbush B, Isenring P, Schulte PM. Changes in gene expression in gills of the
644 euryhaline killifish Fundulus heteroclitus after abrupt salinity transfer. Am J Physiol Cell Physiol.
645 2004;287:C300-C309. doi:10.1152/ajpcell.00054.2004.
646 45. Xu Z, Gan L, Li T, Xu C, Chen K, Wang X, et al. Transcriptome profiling and molecular pathway
647 analysis of genes in association with salinity adaptation in Nile tilapia Oreochromis niloticus. PLoS One.
648 2015;10:e0136506. doi:10.1371/journal.pone.0136506.
649 46. Gibbons TC, Metzger DCH, Healy TM, Schulte PM. Gene expression plasticity in response to salinity
650 acclimation in threespine stickleback ecotypes from different salinity habitats. Mol Ecol. 2017;26:2711-
651 2725. doi:10.1111/mec.14065.
652 47. Ron D, Walter P. Signal integration in the endoplasmic reticulum unfolded protein response. Nat Rev
653 Mol Cell Biol. 2007;8:519-529. doi:10.1038/nrm2199.
654 48. Hetz C. The unfolded protein response: controlling cell fate decisions under ER stress and beyond. Nat
655 Rev Mol Cell Biol. 2012;13:89-102. doi:10.1038/nrm3270.

656 49. Kültz D. Molecular and evolutionary basis of the cellular stress response. Annu Rev Physiol.
657 2005;67:225-257. doi:10.1146/annurev.physiol.67.040403.103635.
658 50. Schröder M, Kaufman RJ. The mammalian unfolded protein response. Annu Rev Biochem. 2005;74:739-
659 789. doi:10.1146/annurev.biochem.73.011303.074134.
660 51. Hetz C, Papa FR. The unfolded protein response and cell fate control. Mol Cell. 2018;69:169-181.
661 doi:10.1016/j.molcel.2017.06.017.
662 52. Duffy NM, Bui P, Bagherie-Lachidan M, Kelly SP. Epithelial remodeling and claudin mRNA abundance
663 in the gill and kidney of puffer fish (Tetraodon biocellatus) acclimated to altered environmental ion levels. J
664 Comp Physiol B. 2011;181:219-238. doi:10.1007/s00360-010-0517-3.
665 53. Notch EG, Shaw JR, Coutermarsh BA, Dzioba M, Stanton BA. Morpholino gene knockdown in adult
666 Fundulus heteroclitus: role of SGK1 in seawater acclimation. PLoS One. 2011;6:e29462.
667 doi:10.1371/journal.pone.0029462.
668 54. Yamaguchi T, Dijkstra JM. Major histocompatibility complex genes and disease resistance in fish. Cells.
669 2019;8:378. doi:10.3390/cells8040378.
670 55. Tocher DR. Metabolism and functions of lipids and fatty acids in teleost fish. Rev Fish Sci. 2003;11:107-
671 184. doi:10.1080/713610925.
672 56. Polakof S, Panserat S, Soengas JL, Moon TW. Glucose metabolism in fish: a review. J Comp Physiol B.
673 2012;182:1015-1045. doi:10.1007/s00360-012-0658-7.
674 57. Mohd-Padil H, Tajul-Arifin K, Mohd-Adnan A. Characterization of the functional domain of beta-2-
675 microglobulin from the Asian seabass, Lates calcarifer. PLoS One. 2010;5:e13159.
676 doi:10.1371/journal.pone.0013159.
677 58. Rodrigues PN, Vazquez-Dorado S, Neves JV, Wilson JM. Dual function of fish hepcidin: response to
678 experimental iron overload and bacterial infection in sea bass (Dicentrarchus labrax). Dev Comp Immunol.
679 2006;30:1156-1167. doi:10.1016/j.dci.2006.02.005.
680 59. Li YY, Hu CB, Zheng YJ, Xia XA, Xu WJ, Wang SQ, et al. The effects of dietary fatty acids on liver
681 fatty acid composition and Delta(6)-desaturase expression differ with ambient salinities in Siganus
682 canaliculatus. Comp Biochem Physiol B Biochem Mol Biol. 2008;151:183-190.
683 doi:10.1016/j.cbpb.2008.06.013.

684 60. Bar-Joseph Z, Gitter A, Simon I. Studying and modelling dynamic biological processes using time-series
685 gene expression data. Nat Rev Genet. 2012;13:552-564. doi:10.1038/nrg3244.
686 61. Whitmore D, Foulkes NS, Strähle U, Sassone-Corsi P. Light acts directly on organs and cells in culture
687 to set the vertebrate circadian clock. Nature. 2000;404:87-91. doi:10.1038/35003589.
688 62. Isorna E, de Pedro N, Valenciano AI, Alonso-Gómez ÁL, Delgado MJ. Interplay between the endocrine
689 and circadian systems in fishes. J Endocrinol. 2017;232:R141-R159. doi:10.1530/JOE-16-0330.
690 63. Frøland Steindal IA, Whitmore D. Circadian clocks in fish—what have we learned so far? Biology.
691 2019;8:17. doi:10.3390/biology8010017.
692 64. Sánchez-Bretaño A, Alonso-Gómez ÁL, Delgado MJ, Isorna E. The liver of goldfish as a component of
693 the circadian system: integrating a network of signals. Gen Comp Endocrinol. 2015;221:213-216.
694 doi:10.1016/j.ygcen.2015.05.001.
695 65. Boyle G, Richter K, Priest HD, Traver D, Mockler TC, Chang JT, et al. Comparative analysis of
696 vertebrate diurnal/circadian transcriptomes. PLoS One. 2017;12:e0169923.
697 doi:10.1371/journal.pone.0169923.
698 66. Conesa A, Madrigal P, Tarazona S, et al. A survey of best practices for RNA-seq data analysis. Genome
699 Biol. 2016;17:13. doi:10.1186/s13059-016-0881-8.
700 67. Soneson C, Love MI, Robinson MD. Differential analyses for RNA-seq: transcript-level estimates
701 improve gene-level inferences. F1000Res. 2015;4:1521. doi:10.12688/f1000research.7563.2.
702 68. Percie du Sert N, Hurst V, Ahluwalia A, et al. The ARRIVE guidelines 2.0: updated guidelines for
703 reporting animal research. PLoS Biol. 2020;18:e3000410. doi:10.1371/journal.pbio.3000410.

Supplementary Files

This is a list of supplementary files associated with this preprint. Click to download.

- BMCGenomicsSupplementary11226.docx